

## Detection of the Early Stage of Recombinational DNA Repair by Silicon Nanowire Transistors

Marco Chiesa,<sup>†</sup> Paula P. Cardenas,<sup>‡</sup> Francisco Otón,<sup>§</sup> Javier Martinez,<sup>†</sup> Marta Mas-Torrent,<sup>§</sup> Fernando Garcia,<sup>†</sup> Juan C. Alonso,<sup>‡</sup> Concepció Rovira,<sup>§</sup> and Ricardo Garcia\*,<sup>†</sup>

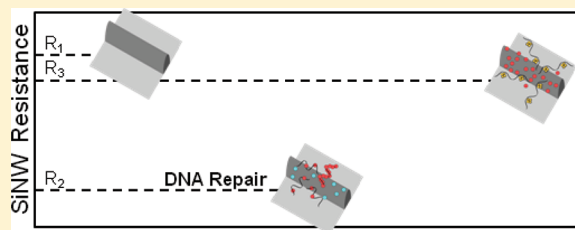
<sup>†</sup>Instituto de Microelectrónica de Madrid (IMM-CNM-CSIC), Isaac Newton 8, 28760 Tres Cantos, Madrid, Spain

<sup>‡</sup>Centro Nacional de Biotecnología (CNB-CSIC), Darwin 3, 28049 Madrid, Spain

<sup>§</sup>Institut de Ciència de Materials de Barcelona (ICMAB-CSIC) and CIBER-BBN, Campus Universitari de Bellaterra, Cerdanyola, 08193 Barcelona, Spain

**ABSTRACT:** A silicon nanowire-based biosensor has been designed and applied for label-free and ultrasensitive detection of the early stage of recombinational DNA repair by RecA protein. Silicon nanowire transistors were fabricated by atomic force microscopy nanolithography and integrated into a microfluidic environment. The sensor operates by measuring the changes in the resistance of the nanowire as the biomolecular reactions proceed. We show that the nanoelectronic sensor can detect and differentiate several steps in the binding of RecA to a single-stranded DNA filament taking place on the nanowire–aqueous interface. We report relative changes in the resistance of 3.5% which are related to the interaction of 250 RecA–single-stranded DNA complexes. Spectroscopy data confirm the presence of the protein–DNA complexes on the functionalized silicon surfaces.

**KEYWORDS:** Silicon nanowires transistors, AFM oxidation nanolithography, protein–DNA, RecA, presynapsis



The high surface-to-volume ratio and the small size of silicon nanowires (SiNWs)<sup>1</sup> make them appealing candidates to fabricate a variety of ultrasensitive devices.<sup>2,3</sup> The applications space from (bio)chemical sensors<sup>4–6</sup> to electromechanical resonators<sup>7</sup> or optical sensors.<sup>8,9</sup> In particular, it has been proposed to use SiNWs as label-free biosensors<sup>10,11</sup> to detect nucleic acids,<sup>11–13</sup> antigen–antibody interactions,<sup>11,14,15</sup> virus–antibody binding,<sup>16</sup> and small molecule–protein interactions.<sup>17</sup> Silicon nanowires can be fabricated by using both bottom-up and top-down approaches. Bottom-up methods are based on a catalyst-assisted growth.<sup>2,3</sup> Those methods are able to generate very small nanowires with diameters below 5 nm.

On the other hand, top-down approaches are based on optical,<sup>14</sup> electron beam,<sup>18</sup> or atomic force microscopy (AFM) lithographies<sup>19</sup> and allow placing nanowires with accuracies comparable with the device size.<sup>13,15,19</sup> In particular, AFM oxidation nanolithography has shown the ability to fabricate SiNW field-effect transistors with sub-10 nm channel widths, and at the same time, the nanolithography has the ability to position the SiNWs with sub-100 nm accuracy.<sup>15,19</sup> Furthermore, AFM-based nanolithography is compatible with complementary metal oxide semiconductor technology (CMOS).

The RecA family of ATPases (RecA/RadA/Rad51/DMC1) mediates homologous recombination (HR), a reaction essential for maintaining genomic integrity and for generating genetic diversity in all living organisms.<sup>20–22</sup> The broad spectrum of biological functions cannot be attributed to the action of an individual monomer. Bacterial RecA, which is a 38 kDa protein

with a diameter of  $\sim 27$  Å,<sup>23</sup> binds (deoxy)adenosine triphosphate ((d)ATP) and a divalent cation (i.e., Mg<sup>2+</sup>) at the monomer interface to complex with single-stranded (ss) DNA and form active and dynamic right-handed nucleoprotein filaments.<sup>24–27</sup> The formation of a polymorphic right-handed helix of RecA around the DNA, with  $\sim 6$  monomers per helix turn (1 RecA monomer/3 nucleotides [nt]), provides a large surface where homology can be measured and matched with complementary partner and where DNA structural transitions can be cooperatively transmitted over long distance. The RecA·(d)ATP and RecA·ssDNA interactions, which are allosterically coupled, induce new RecA·RecA interfaces that activate the RecA·ssDNA filaments for HR.<sup>24–27</sup> To disassemble the RecA·ssDNA filaments, (d)ATP hydrolysis is needed.<sup>20–22</sup> The assemble process is regulated at multiple levels by mediators and modulators.<sup>27</sup> Among them, a single-stranded binding protein (SSB or SsbA) competes with RecA for binding to ssDNA and thereby prevents unwanted HR.<sup>27–30</sup>

Here, we apply SiNWs transistors, fabricated by AFM oxidation nanolithography, to detect the interaction processes between ssDNA and a RecA-bound dATP, involved in the catalysis of DNA strand exchange, an essential step during homologous recombination. The narrow channel width and the high surface-to-volume ratio of the nanowires give them

**Received:** October 25, 2011

**Revised:** January 23, 2012

**Published:** February 24, 2012

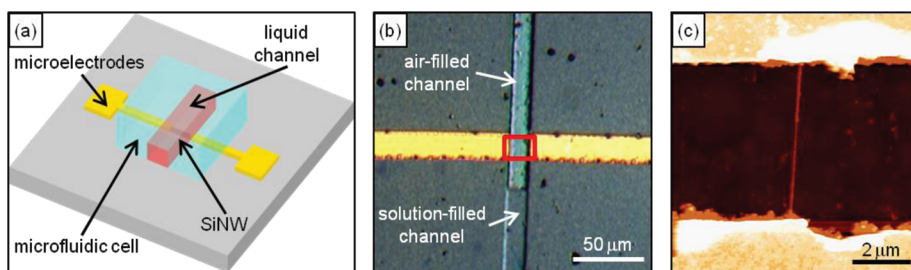


**Figure 1.** (a) Scheme of the device setup that includes the microfluidic cell. (b) Optical micrograph of the microfluidic channel, gold microcontacts, and nanowire region that bridges the Au contacts. The change in contrast in the channel indicates the regions filled (dark) or unfilled (bright) with the protein solution. (c) AFM image of the device active area (red rectangle of (b)) taken after several biosensing measurements.

enough sensitivity to detect the dynamic interactions of RecA at the dATP-RecA-ssDNA complex. We show that SiNW devices can detect and differentiate among the different biomolecular processes taking place in the SiNW-liquid interface by measuring the changes in the resistance of the nanowire as the biomolecular reactions proceed. In particular, the SiNW differentiates the binding of RecA to ssDNA, from the situation where there is a competition between RecA and another protein SsbA for the binding sites along the DNA chain. In the latter case, the dATPase activity of RecA is inhibited because the RecA-ssDNA filaments are not formed. The SiNW device is very sensitive; specifically, the observed changes are related to the interaction of about 250 DNA-protein complexes.

Figure 1 shows a scheme of the SiNW biosensor together with optical and AFM micrographs of one of the devices used in these experiments (Figure 1b,c). The experiments were performed by measuring the current-voltage ( $I$ - $V$ ) curves of the SiNW fabricated by AFM oxidation nanolithography. The resistance of the nanowire was found to change depending on the nature of the analyte solution surrounding it. The analytes in the solution were passed through a microfluidic channel of  $20\ \mu\text{m}$  width and  $3\ \mu\text{m}$  height which runs across the active surface of the nanowire device. We have used six different environments through the microfluidics cell, listed as no solution (dry), biological buffer, RecA, RecA + dATP, RecA + dATP + ssDNA, and ssDNA + SsbA + RecA + dATP. The last solution is intended as a critical control experiment because SsbA is expected to compete against RecA to bind to ssDNA and indirectly inhibit the dATPase activity of RecA.<sup>28,31</sup>

Figure 2 shows different schemes of the molecules relevant here. Parts a, b, and c of Figure 2 show respectively a RecA-dATP complex, dATP, and SsbA. The attachment of RecA to ssDNA is shown in Figure 2d while the attachment of a competing molecule such as SsbA is shown in Figure 2e, and the displacement mechanism is shown in Figure 2f.

The typical output characteristics of the SiNWs are shown in Figure 3. Figure 3a shows the  $I$ - $V$  curves of a bare SiNW that has not been exposed to any liquid solution. The curves show a quasi-linear dependence with the drain-to-source voltage. The application of a positive gate voltage increases the slope of the curves, which translates into a smaller effective resistance. The change in the resistance with the gate voltage is crucial to explain the behavior of the SiNW biomolecular sensor. From these data, a threshold voltage  $V_{\text{th}} = -10.8\ \text{V}$  can be extrapolated. From the AFM images such as the one shown in Figure 1c and the tip's curvature radius, the length  $L$ , the width  $W$ , and the height  $h$  of the nanowire can be determined. In particular, for the sensor of Figure 3, we have obtained  $5\ \mu\text{m}$ ,  $90\ \text{nm}$ , and  $28\ \text{nm}$  respectively for  $L$ ,  $W$ , and  $h$ . From the

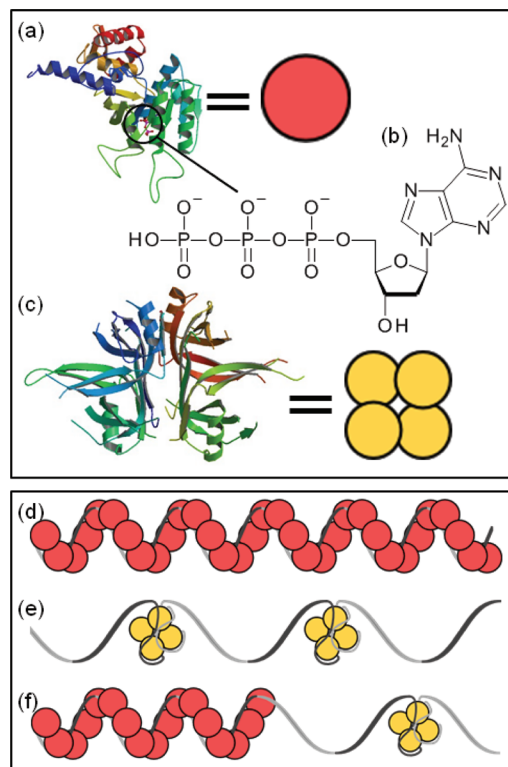


**Figure 2.** Scheme of some of the molecules used in this study and of their binding to ssDNA. (a) Image of RecA-bound dATP complex obtained from the RCSB PDB<sup>32</sup> and its schematic representation. The circle highlights dATP. (b) Chemical formula of dATP. (c) Image of the SSB obtained from the RCSB PDB<sup>33</sup> and its schematic representation. (d) Scheme of a RecA-ssDNA filament. (e) Scheme of the SsbA-ssDNA complex. (f) Scheme of ssDNA bound RecA and SsbA.

geometry and the measured threshold voltage, we can extract a gate-nanowire capacitance of  $0.10\ \text{fF}$  and a total mobile charge in the nanowire of about  $7 \times 10^3$  electrons at zero gate voltage by using a parallel capacitor geometry for the gate-insulator-nanowire interface

$$C = \frac{Q}{V_{\text{th}}} = \epsilon_{\text{ox}} \frac{LW}{d} \quad (1)$$

where  $\epsilon_{\text{ox}}$  and  $d$  are respectively the dielectric constant and the thickness of the silicon dioxide within the silicon-on-insulator (SOI) substrate.

In a first approximation, the conductance of the nanowire is proportional to the number of mobile carriers present. Therefore, a 1% decrease in the device resistance indicates

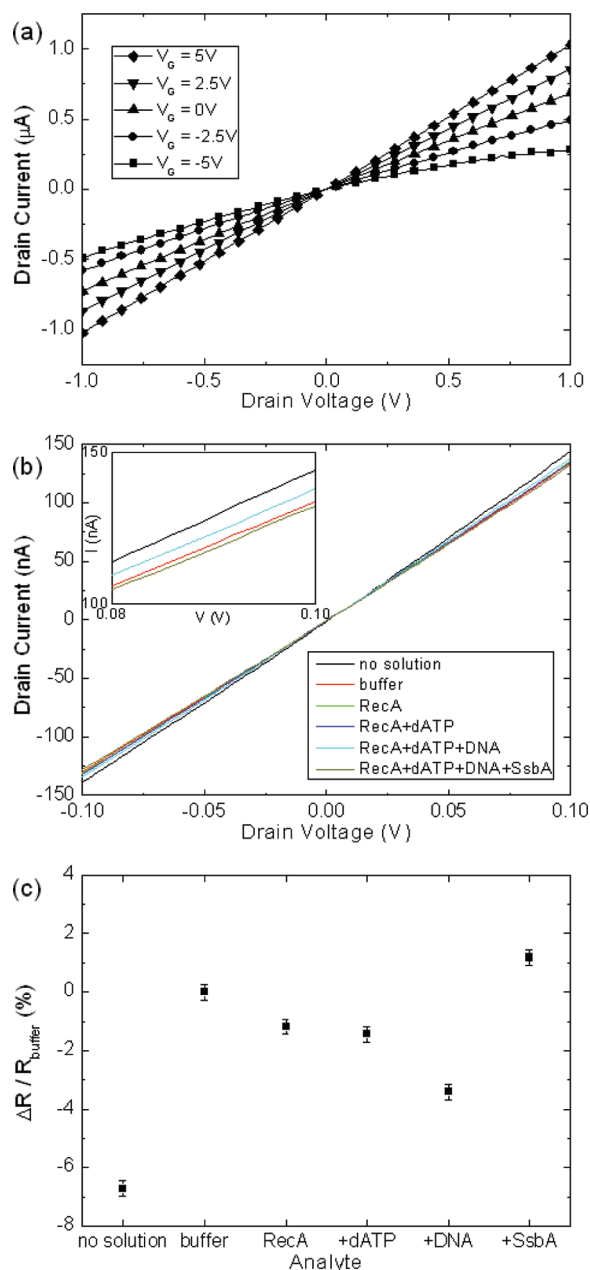
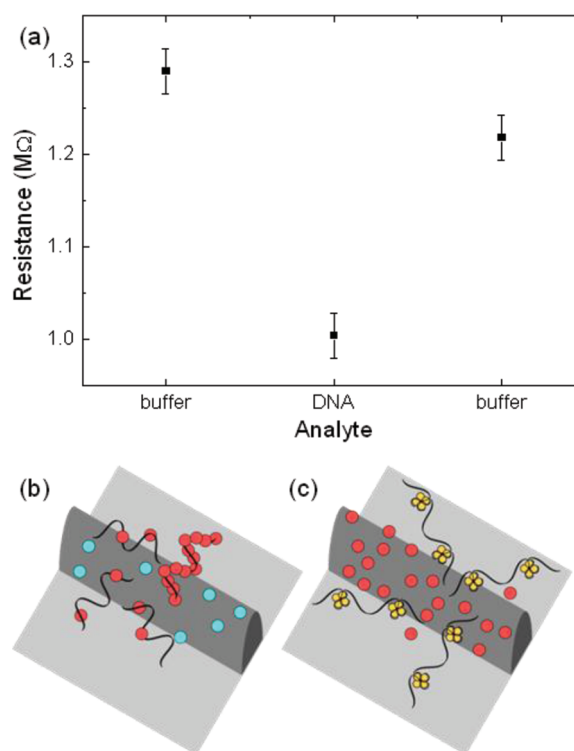


**Figure 3.** (a) Output characteristic curves of a SiNW transistor (back-gated). The device behaves like a n-channel FET with a threshold voltage of about  $-10.8$  V. (b)  $I$ – $V$  curves of a SiNW exposed to different solutions. Note that the relation is always linear. The inset shows a magnification of the curves in the interval (0.08–0.1 V) to highlight the differences. (c) Response of the biomolecular SiNW sensor to the different analytes. The nanowire is not functionalized.

that 70 electrons have been induced in the nanowire by the analyte. Upon exposure to different buffer solutions, the output curves of the device are modified (Figure 3b). A clear representation of the process is achieved by plotting the inverse slope of the curves (i.e., the effective resistance  $R$ ) as it is shown in Figure 3c. This plot shows that, upon exposure to the solutions, the resistance of the device changes. Interestingly, not only the resistance of the SiNW device depends on the liquid environment but also the differences among them are greater than the noise of the device. The minimum resistance is observed when the RecA–ssDNA filaments are formed in presence of dATP. The resistance is 3.5% lower than the

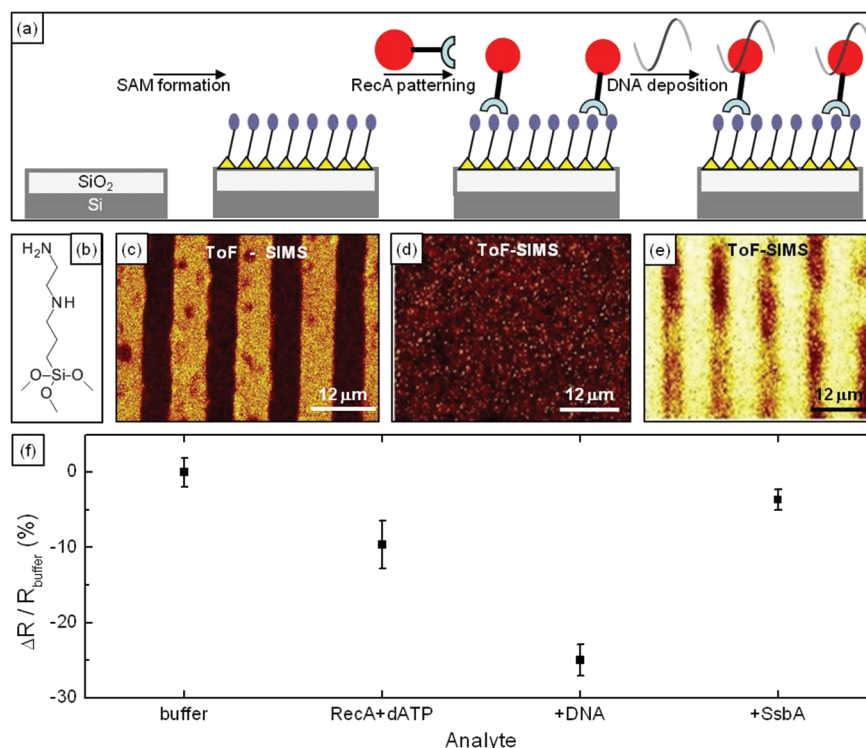
experiment performed with pure buffer. This result indicates that about 250 electrons have been induced in the nanowire. It is important to remember that in these conditions the energy provided by the hydrolysis of dATP into deoxyadenosine diphosphate (dADP) and inorganic phosphate (Pi) is needed to disassemble the RecA from the ssDNA. As a consequence, the concentration of dADP molecules increases. For this reason, it is possible to associate the observed changes with the molecular disassembly of the protein from ssDNA. The error bars represent the range of resistances measured in subsequent experiments under the same environment. The typical error is  $\pm 0.3\%$ , which gives a sensitivity limit of about 20 electrons.

Figure 4a shows changes in the resistance before, during, and after the SiNW were exposed to the sequence of solutions



**Figure 4.** (a) Reversibility in the operation point of the SiNW biomolecular sensor. The resistance of the same device was measured in buffer A and then exposed to a solution containing RecA–ssDNA and dATP, and finally the SiNW was cleaned by flushing with water and buffer A to remove the unbound analyte and measured again in buffer A. (b) Scheme of the electrostatic charge environment in the proximity of SiNW in the presence of RecA and ssDNA. (c) Scheme of the electrostatic charge environment in the proximity of the sensor in the presence of RecA, ssDNA, and SsbA. Red and blue dots represent RecA complexed with dATP and dADP, respectively.

containing RecA, RecA + dATP, and RecA + dATP + ssDNA. The SiNW nearly recovers its initial resistance once the biomolecular processes have been stopped (rinsing of the SiNW in water and buffer). This indicates that the detection process does not introduce significant changes in the electronic structure of the nanowire. Consequently, the electrostatic charges associated with the biomolecular reactions play the role of an effective gate voltage. To avoid any influence of the pH in the measurements, the same  $\text{pH} = 7$  has been used in all the measurements and solutions. On the other hand, the sensitivity of the SiNW to the electrical charge of the medium has been



**Figure 5.** (a) Scheme of the surface functionalization and the immobilization of RecA and ssDNA. (b) Chemical formula of the functionalizing agent *N*-(1-trimethoxysilylpropyl)ethylenediamine. (c) Sum ToF-SIMS image of the RecA pattern. The bright stripes show a strong presence of amino acids-related fragments and thus RecA. (d, e) ToF-SIMS images of phosphate anion ( $\text{PO}_3^-$ ) in the RecA-functionalized surface without (d) and with DNA (e). The bright areas correspond to the areas where  $\text{PO}_3^-$  ion is found and thus RecA-ssDNA complexes. (f) Response of the functionalized biomolecular SiNW sensor to the different analyte solutions.

calibrated by changing the pH from basic to acid. In this way we have determined that an excess of positive charge in vicinity of the SiNW sensor produces an increase of the resistance. Figure 4b,c shows a scheme of the distribution of the relevant molecules in the vicinity of the nanowire in two conditions: (i) the solution contains dATP, ssDNA, and limiting RecA (1 RecA monomer per 15-nt) (Figure 4b) and (ii) RecA and dATP have been added to a solution of preassembled ssDNA and SsbA (1 SsbA tetramer per 60-nt) (Figure 4c).

The response of the SiNW sensor to the different analytes can be explained in terms of the relevant biomolecular reactions. First of all, the transistor characteristics (Figure 3a) indicate that the conduction is electronic (n-channel). Therefore, a decrease of the wire resistance indicates an increase of the electron density in the wire, which is induced by the increase of the concentration of positive charges (or by a reduction of the negative charges) in the vicinity of the SiNW. For this reason, we expect the current in the nanowire to increase when the RecA-dATP complexes in the vicinity of the nanowire lose one negatively charged phosphate group by hydrolysis of dATP (which is converted into dADP + Pi), thus generating a RecA-dADP complex. Since the phosphate groups of dATP have a negative charge, the loss of one of them reduces the negative charge around the wire and therefore the wire resistance.

The above findings are consistent with the biochemistry of these complexes. The low dissociation constants of the complexes between RecA and a nucleotide such as dATP or dADP (the product of dATP hydrolysis), in physiological conditions the equilibrium is shifted strongly toward the complexed state; i.e., all RecA molecules are bound to a

nucleotide.<sup>30</sup> Therefore, all RecA proteins carry a negative charge which depends on the number of phosphate groups of the bound nucleotide, a RecA-dATP complex being more negatively charged than a RecA-dADP complex.

It is worth mentioning that RecA is a ssDNA-dependent ATPase, and dATP hydrolysis produces dADP, which destabilizes and dissociates RecA from the ssDNA.<sup>27</sup> It is therefore in this situation where we expect the highest concentration of dADP in the solution and in the vicinity of the nanowire. This is consistent with the observed decrease of the nanowire resistance when ssDNA is added to the RecA-dATP complex. It is important to remark that the overall charge of the solution does not vary during the biomolecular reaction. However, for the SiNW sensor the charged species situated in the proximity of the nanowire are the ones that affect the carrier density, i.e., the resistance or the conductivity. The results indicate that RecA is deposited on the nanowire surface, while the phosphate groups are more uniformly distributed within the solution. The role of SsbA, on the other hand, is less straightforward. If SsbA is preincubated with ssDNA, RecA loading onto ssDNA is inhibited and the consequent dATPase activity of RecA is reduced. The apparent inconsistency of the sensor response, observed when RecA, dATP, ssDNA, and SsbA were added at the same time, could be explained by the observation that, if SsbA is added to a solution after RecA, it melts the secondary structures present in the ssDNA, thereby increases the binding of RecA to ssDNA and stimulates the (d)ATPase activity of RecA.<sup>28</sup>

In order to test the mechanism and increase the sensitivity of the SiNWs biosensor, we functionalized the surface of the nanowire with an amine-terminated self-assembled monolayer

(SAM) (Figure 5a) formed with *N*-(1-trimethoxysilylpropyl)-ethylenediamine (Figure 5b). This molecule was chosen because of the favorable interaction that can be established by the SAM amine groups and several amino acid residues placed in the outer surface of the RecA that are not implicated in the binding to ssDNA. Indeed, the ATPase activity of SAM-derivatized RecA was similar to wild-type RecA (data not shown). In this way a higher concentration of RecA in the vicinity of the active area of the sensor should be obtained. Previous to the SiNWs experiments, the activity of RecA and the specific interactions were tested in a micrometer surface. All surfaces were characterized by XPS and time of flight secondary ion mass spectroscopy (ToF-SIMS) after rinsing them with Milli-Q water. The spectroscopy experiments performed over a patterned functionalized area of a silicon oxide wafer showed the preferential deposition of ssDNA over RecA protein.

Figure 5c shows the ToF-SIMS map (sum of the amino acid-related peaks) after deposition of RecA.<sup>34</sup> In this image the brighter stripes show the sum of the individual contributions from amino acids-related fragments such as  $C_2H_4N^+$  (which is associated with the presence of alanine, glycine, histidine, leucine, serine),  $C_3H_6N^+$  (which is associated with lysine, methionine, valine), and  $C_4H_6NO^+$  (associated with glutamine, glutamic acid). The individual signals also show the presence of the line pattern. Figure 5d,e shows the ToF-SIMS map at the phosphate group peak before and after depositing ssDNA on the surface patterned with RecA. The bright areas correspond to the areas where  $PO_3^-$  ion is found. Thus, the images show that RecA binds to the derivatized surface and that it is still able to bind ssDNA. Figure 5f shows the response of the sensor functionalized with *N*-(1-trimethoxysilylpropyl)-ethylenediamine. By comparing these results with those obtained on the unfunctionalized sensor (Figure 3c), we can observe a stronger response to the detection of the binding of RecA and ssDNA. This is due to the higher concentration of RecA on the nanowire-functionalized surface and indicates that the immobilization by the SAM does not result in a steric hindrance of the functionality of RecA.

In short, we have designed a label-free and ultrasensitive biosensor based on monitoring the changes in the resistance of a silicon nanowire transistor. The biosensor has been fabricated by AFM lithography, and it has been integrated into a microfluidic cell. This nanoelectronic sensor has been applied to the measure the early stages of recombinational DNA repair by RecA protein. Specifically, the SiNW device is able to detect the biomolecular processes related to the dATP hydrolysis required for dissociation of RecA from ssDNA—which define the early stage of RecA-mediated homologous recombination—and the inhibition of this activity when a competing protein, SsbA, is present. We have shown that the interaction of 250 RecA molecules can be detected.

**Experimental Section.** *AFM Oxidation Nanolithography.* The nanowire masks were defined using a dynamic AFM operated in the low-amplitude solution (noncontact) with additional circuits to perform the oxidation.<sup>15,19,35,36</sup> The microscope was placed into a closed box with inlets for dry and water vapor-saturated nitrogen. The relative humidity in the AFM chamber was kept above 50%. Noncontact AFM oxidation was performed with doped  $n^+$ -type silicon cantilevers (Veeco). The force constant  $k$  and the resonant frequency  $f_0$  were about  $30 \text{ N m}^{-1}$  and 300 kHz, respectively. The cantilever was excited at its resonant frequency. The nanowire mask was

defined by applying pulses of 18–30 V amplitude and 100  $\mu\text{s}$ –10 ms duration with 5–10 nm separation.

*Fabrication of Silicon Nanowire Transistors.* Silicon nanowire devices were fabricated by AFM oxidation on silicon-on-insulator (SOI) wafers with a 57 nm Si active layer and a 151 nm buried oxide layer (IBIS Technology, Danvers, MA). Phosphorus was implanted to achieve a resistivity of 0.01–0.025  $\Omega \text{ cm}$ . The implantation was performed in the ICTS Sala Blanca (IMB-CNM, Spain). The SOI substrates were cleaned by three ultrasonic bath cycles in  $\text{NH}_4\text{OH}/\text{H}_2\text{O}_2/\text{H}_2\text{O}$  (1:1:2) for 12 min each, then sonicated in deionized water (5 min), and blown dry in  $\text{N}_2$ . Successively, Cr–Au markers were defined by photolithography. Local oxidation nanolithography was then employed to write a 3 nm thick  $\text{SiO}_2$  mask which defines the nanowire.<sup>19</sup> A second photolithography and Cr–Au evaporation step was then used to define the channel length of the silicon nanowire device and to provide the source and drain contacts of the nanowire. For sake of simplicity, the substrate is used as a back-gate electrode. Finally, the unmasked silicon was removed by reactive ion etching (RIE) with a plasma comprised of 80%  $\text{SF}_6$  and 20%  $\text{O}_2$  (PlasmaLab 80, Oxford Instruments, UK). The etching time is around 10 s. Typical dimensions of the silicon nanowire were 5–10  $\mu\text{m}$  for the length, 50–100 nm for the width, and 30–50 nm for the height.

*Microfluidic Cells.* A master for microfluidic cells with a section of  $20 \times 3 \mu\text{m}^2$  was fabricated by photolithography on a microscope slide which was previously cleaned in an  $\text{O}_2$  plasma etcher for 5 min at 50 W rf power. Polydimethylsiloxane (PDMS) microfluidic cells were fabricated by pouring a 10:1 mixture of Sylgard-184 silicone elastomer and Sylgard-184 silicon elastomer curing agent (Dow Corning) over the master in a Petri dish. Then, the Petri dish was baked at 90  $^\circ\text{C}$  for 45 min. The cured PDMS was peeled off the master and then cut to the final cell size. Prior to their use, the cells were made more hydrophilic by exposing them to oxygen plasma (50 W, 30 s). The cells were successively aligned onto the transistor channel under an optical microscope.

*Proteins and Solutions.* The reactions between the analytes are performed in a buffer A (Tris-HCl 50 mM (pH = 7), NaCl 40 mM, Mg acetate  $\text{Mg}(\text{OAc})_2$  10 mM, dithiothreitol (DTT) 1 mM, bovine serum albumin (BSA) 50  $\mu\text{g mL}^{-1}$ ). The ssDNA is diluted in buffer A. The typical concentrations in the reaction volume are dATP 2 mM, ssDNA 9  $\mu\text{M}$  (3000-nt pGEM circular ssDNA, in nucleotide), RecA 0.6  $\mu\text{M}$  (in monomers), and SsbA 0.15  $\mu\text{M}$  (in tetramers). *B. subtilis* RecA and SsbA proteins were purified as previously described.<sup>29</sup>

*Surface Functionalization.* The formation of the amine-terminated SAM has been carried out putting the  $\text{SiO}_x$  surface in contact with a 0.1% solution of the silane in dry toluene during 3 h or by vapor deposition of the silane in vacuum. Then the surface is washed with HPLC grade toluene and ethanol and dried with a nitrogen flow. Both methodologies give similar results. Nanowire functionalization was performed by vapor deposition of the silane in vacuum. After removing it from the solution, the surface was rinsed several times with 5 mL of Milli-Q water and dried with nitrogen. The presence of the RecA on the surface was confirmed by contact angle, AFM, and XPS. The value of contact angle undergoes an increase from 60 $^\circ$  to 80 $^\circ$ . Moreover, AFM images texture changes exhibiting a larger roughness (11.6 nm) and grain size due to the formation of aggregates of the protein. The most important evidence is the XPS spectrum in which a significant change in the C, N,

and O profile is observed. Protein immobilization was achieved both by immersion of the SAM in a solution of the protein ( $c = 10 \mu\text{M}$  in buffer A) for 16 h at room temperature or by microcontact printing. For the microcontact printing of the protein striped polydimethylsiloxane (PDMS) stamps were used with 6 or 20  $\mu\text{m}$  width. The stamp was introduced in the solution for 45 min. Then, the stamp was extracted from the solution and dried with a nitrogen flow, and then the stamp was pressed manually for 1 min on the SAM-modified surface. Excess material was then removed by rinsing several times in 5 mL of Milli-Q water and dried with nitrogen. The RecA used is a 1 mg mL<sup>-1</sup> solution in NaCl 300 mM, Tris-HCl 50 mM, 10% glycerol buffer. Dilutions of the sample were done in buffer A containing 1 nM dATP. Two different ssDNA were used: pGEM-3Z(+) and poly dT. Concentrations of the sample from  $c = 0.01$  to 0.5 mg mL<sup>-1</sup> were used.

**Electrical Characterization.** Current–voltage ( $I$ – $V$ ) characteristics of the nanowire transistors were measured with a HP4145B semiconductor parameter analyzer connected to a Karl Süss probe station. The different solutions were passed through the microfluidic cell driven by capillarity, taking care not to create parasitic paths between the electrodes outside the cell. When measuring solutions, the gate electrode is left floating in order to reduce leakage currents.

## AUTHOR INFORMATION

### Corresponding Author

\*E-mail: ricardo.garcia@imm.cnm.csic.es.

### Notes

The authors declare no competing financial interest.

## ACKNOWLEDGMENTS

This work was made possible by the CSIC through its interdisciplinary collaborative program (PIF08-008). We also acknowledge the partial financial support from the Ministerio de Ciencia, Investigación e Innovación (MAT2009-08650 and CTQ2010-195011/BQU), the Generalitat de Catalunya (2009SGR00516), and the CIBER de Bioingeniería, Biomateriales y Nanomedicina (CIBER-BBN), promoted by ISCIII, Spain; M.C. and F.O. acknowledge the program “Juan de la Cierva” (MICINN).

## REFERENCES

- Rurali, R. Colloquium: Structural, Electronic, and Transport Properties of Silicon Nanowires. *Rev. Mod. Phys.* **2010**, *82*, 427–449.
- Xia, Y.; Yang, P.; Sun, Y.; Wu, Y.; Mayers, B.; Gates, B.; Yin, Y.; Kim, F.; Yan, H. One-Dimensional Nanostructures: Synthesis, Characterization, and Applications. *Adv. Mater.* **2003**, *15*, 353–389.
- Cui, Y.; Wei, Q.; Park, H.; Lieber, C. M. Nanowire Nanosensors for Highly Sensitive and Selective Detection of Biological and Chemical Species. *Science* **2001**, *293*, 1289–1292.
- Talin, A. A.; Hunter, L. L.; Léonard, F.; Rokad, B. Large Area, Dense Silicon Nanowire Array Chemical Sensors. *Appl. Phys. Lett.* **2006**, *89*, 153102.
- Leão, C. R.; Fazzio, A.; da Silva, A. J. R. Si Nanowires as Sensors: Choosing the Right Surface. *Nano Lett.* **2007**, *7*, 1172–1177.
- Luo, L.; Jie, J.; Zhang, W.; He, Z.; Wang, J.; Yuan, G.; Zhang, W.; Wu, L. C. M.; Lee, S.-T. Silicon Nanowire Sensors for Hg<sup>2+</sup> and Cd<sup>2+</sup> Ions. *Appl. Phys. Lett.* **2009**, *94*, 193101.
- Feng, X. L.; He, R.; Yang, P.; Roukes, M. L. Very High Frequency Silicon Nanowire Electromechanical Resonators. *Nano Lett.* **2007**, *7*, 1953–1959.
- Mu, L.; Shi, W.; Chang, J. C.; Lee, S.-T. Silicon Nanowires-Based Fluorescence Sensor for Cu(II). *Nano Lett.* **2008**, *8*, 104–109.
- Servati, P.; Colli, A.; Hofmann, S.; Fu, Y. Q.; Beecher, P.; Durrani, Z. A. K.; Ferrari, A. C.; Flewitt, A. J.; Robertson, J.; Milne, W. I. Scalable Silicon Nanowire Photodetectors. *Physica E* **2007**, *38*, 64–66.
- Chen, K.-I.; Li, B.-R.; Chen, Y.-T. Silicon Nanowire Field-Effect Transistor-Based Biosensors for Biomedical Diagnosis and Cellular Recording Investigation. *Nano Today* **2011**, *6*, 131–154.
- Zheng, G.; Patolsky, F.; Cui, Y.; Wang, W. U.; Lieber, C. M. Multiplexed Electrical Detection of Cancer Markers with Nanowire Sensor Arrays. *Nat. Biotechnol.* **2005**, *23*, 1294–1301.
- Hahm, J.-i.; Lieber, C. M. Direct Ultrasensitive Electrical Detection of DNA and DNA Sequence Variations Using Nanowire Nanosensors. *Nano Lett.* **2004**, *4*, 51–54.
- Gao, A.; Lu, N.; Dai, P.; Li, T.; Pei, H.; Gao, X.; Gong, Y.; Wang, Y.; Fan, C. Silicon-Nanowire-Based CMOS-Compatible Field-Effect Transistor Nanosensors for Ultrasensitive Electrical Detection of Nucleic Acids. *Nano Lett.* **2011**, *11*, 3974–3978.
- Stern, E.; Klemic, J. F.; Routenberg, D. A.; Wyrembak, P. N.; Turner-Evans, D. B.; Hamilton, A. D.; LaVan, D. A.; Fahmy, T. M.; Reed, M. A. Label-Free Immunodetection with CMOS-Compatible Semiconducting Nanowires. *Nature* **2007**, *445*, 519–522.
- Martinez, R. V.; Martinez, J.; Garcia, R. Silicon nanowire circuits fabricated by AFM oxidation nanolithography. *Nanotechnology* **2010**, *21*, 245301.
- Patolsky, F.; Zheng, G.; Hayden, O.; Lakadamyali, M.; Zhuang, X.; Lieber, C. M. Electrical Detection of Single Viruses. *Proc. Natl. Acad. Sci. U. S. A.* **2004**, *101*, 14017–14022.
- Wang, W. U.; Chen, C.; Lin, K.-h.; Fang, Y.; Lieber, C. M. Label-Free Detection of Small-Molecule–Protein Interactions by Using Nanowire Nanosensors. *Proc. Natl. Acad. Sci. U. S. A.* **2005**, *102*, 3208–3212.
- Trivedi, K.; Yuk, H.; Floresca, H. C.; Kim, M. J.; Hu, W. Quantum Confinement Induced Performance Enhancement in Sub-5-nm Lithographic Si Nanowire Transistors. *Nano Lett.* **2011**, *11*, 1412–1417.
- Martinez, J.; Martinez, R. V.; Garcia, R. Silicon Nanowire Transistors with a Channel Width of 4 nm fabricated by Atomic Force Microscope Nanolithography. *Nano Lett.* **2008**, *8*, 3636–3639.
- San Filippo, J.; Sung, P.; Klein, H. Mechanism of Eukaryotic Homologous Recombination. *Annu. Rev. Biochem.* **2008**, *77*, 229–257.
- Cox, M. M. Motoring along with the bacterial RecA protein. *Nat. Rev. Mol. Cell Biol.* **2007**, *8*, 127–138.
- Galletto, R.; Amitani, L.; Baskin, R. J.; Kowalczykowski, S. C. Direct Observation of Individual RecA Filaments Assembling on Single DNA Molecules. *Nature* **2006**, *443*, 875–878.
- Lebedev, D. V.; Baitin, D. M.; Islamov, A. Kh.; Kuklin, A. I.; Shalguev, V. Kh.; Lanzov, V. A.; Isaev-Ivanov, V. V. Analytical Model for Determination of Parameters of Helical Structures in Solution by Small Angle Scattering: Comparison of RecA Structures by SANS. *FEBS Lett.* **2003**, *537*, 182–186.
- Chen, Z.; Yang, H.; Pavletich, N. P. Mechanism of Homologous Recombination from the RecA–ssDNA/dsDNA Structures. *Nature* **2008**, *453*, 489–494.
- Joo, C.; McKinney, S. A.; Nakamura, M.; Rasnik, I.; Myong, S.; Ha, T. Real-Time Observation of RecA Filament Dynamics with Single Monomer Resolution. *Cell* **2006**, *126*, 515–527.
- van Loenhout, M. T. J.; van der Heijden, T.; Kanaar, R.; Wyman, C.; Dekker, C. Dynamics of RecA Filaments on Single-Stranded DNA. *Nucleic Acids Res.* **2009**, *37*, 4089–4099.
- Cox, M. M. Regulation of Bacterial RecA Protein Function. *Crit. Rev. Biochem. Mol. Biol.* **2007**, *42*, 41–63.
- Kowalczykowski, S. C.; Krupp, R. A. Effects of *Escherichia coli* SSB protein on the single-stranded DNA-dependent ATPase activity of *Escherichia coli* RecA protein: Evidence that SSB protein facilitates the binding of RecA protein to regions of secondary structure within single-stranded DNA. *J. Mol. Biol.* **1987**, *193*, 97–113.
- Carrasco, B.; Manfredi, C.; Ayora, S.; Alonso, J. C. *Bacillus subtilis* SsbA and dATP regulate RecA nucleation onto single-stranded DNA. *DNA Repair* **2008**, *7*, 990–996.

(30) Watanabe, R.; Masui, R.; Mikawa, T.; Takamatsu, S.; Kato, R.; Kuramitsu, S. Interaction of *Escherichia coli* RecA Protein with ATP and Its Analogues. *J. Biochem.* **1994**, *116*, 960–966.

(31) Roy, R.; Kozlov, A. G.; Lohman, T. M.; Ha, T. SSB protein diffusion on single-stranded DNA stimulates RecA filament formation. *Nature* **2009**, *461*, 1092–1097.

(32) Datta, S.; Krishna, R.; Ganesh, N.; Chandra, N. R.; Muniyappa, K.; Vijayan, M. Crystal Structures of *Mycobacterium smegmatis* RecA and its Nucleotide Complexes. *J. Bacteriol.* **2003**, *185*, 4280–4284.

(33) Savvides, S. N.; Raghunathan, S.; Fütterer, K.; Kozlov, A. G.; Lohman, T. M.; Waksman, G. The C-terminal Domain of Full-Length *E. coli* SSB is Disordered even when Bound to DNA. *Protein Sci.* **2004**, *13*, 1942–1947.

(34) Henry, M.; Bertrand, P. Surface Composition of Insulin and Albumin Adsorbed on Polymer Substrates as Revealed by Multivariate Analysis of ToF-SIMS Data. *Surf. Interface Anal.* **2008**, *41*, 105–113.

(35) Tello, M.; Garcia, R.; Martín-Gago, J. A.; Martínez, N. F.; Martín-González, M. S.; Aballe, L.; Baranov, A.; Gregoratti, L. Bottom-Up Fabrication of Carbon-Rich Silicon Carbide Nanowires by Manipulation of Nanometer-Sized Ethanol Menisci. *Adv. Mater.* **2005**, *17*, 1480–1483.

(36) Calleja, M.; Anguita, J.; Garcia, R.; Birkelund, K.; Pérez-Murano, F.; Dagata, J. A. Nanometre-Scale Oxidation of Silicon Surfaces by Dynamic Force Microscopy: Reproducibility, Kinetics and Nanofabrication. *Nanotechnology* **1999**, *10*, 34–38.